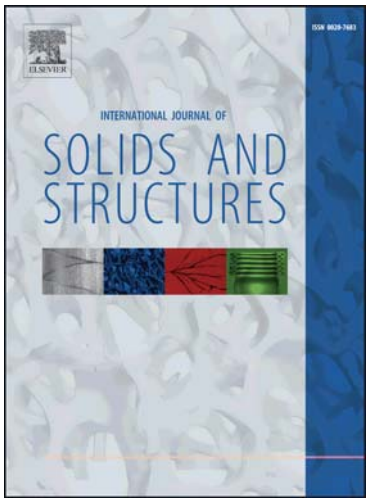

Imperfection-Insensitive Axially Loaded Thin Cylindrical Shells

Xin Ning, Sergio Pellegrino

PII: S0020-7683(15)00002-5
DOI: http://dx.doi.org/10.1016/j.ijsolstr.2014.12.030
Reference: SAS 8611

To appear in: *International Journal of Solids and Structures*

Received Date: 19 November 2013
Revised Date: 2 December 2014
Accepted Date: 30 December 2014

Please cite this article as: Ning, X., Pellegrino, S., Imperfection-Insensitive Axially Loaded Thin Cylindrical Shells, *International Journal of Solids and Structures* (2015), doi: http://dx.doi.org/10.1016/j.ijsolstr.2014.12.030

Imperfection-Insensitive Axially Loaded Thin Cylindrical Shells

Xin Ning, Sergio Pellegrino*

Graduate Aerospace Laboratories, California Institute of Technology
1200 E. California Blvd., Pasadena CA 91125

Abstract

The high efficiency of circular monocoque cylindrical shells in carrying axial loads is impaired by their extreme sensitivity to imperfections and there is an extensive body of literature that addresses this behavior. Instead of following this classical path, focused on circular cross-sections, this paper presents a novel approach that adopts optimal symmetry-breaking wavy cross-sections (wavy shells). The avoidance of imperfection sensitivity is achieved by searching with an evolutionary algorithm for smooth cross-sectional shapes that maximize the minimum among the buckling loads of geometrically perfect and imperfect wavy shells. It is found that shells designed through this approach can achieve higher critical stresses and knockdown factors than any previously known monocoque cylindrical shells. It is also found that these shells have superior mass efficiency to almost all previously reported stiffened shells.

Keywords: Shell buckling, Imperfection-sensitivity, Corrugated shells, Structural optimization, Mass efficiency, Aster shell

1. Introduction

Large discrepancies between analytically predicted and experimentally measured buckling loads for monocoque cylindrical shells were first observed in the 1930's and it was subsequently established that thin cylindrical shells under

*Corresponding author
Email address: sergiop@caltech.edu (Sergio Pellegrino)

axial compression may buckle at loads as low as 20% of the classical value (Brush and Almroth, 1975). Hence, in practice empirically defined knockdown factors are used to decrease the theoretically estimated buckling loads of such shells and this is the currently accepted design approach. Therefore, monocoque cylindrical shells are designed for much larger theoretical buckling loads to ensure that, when the knockdown factor is applied, they still meet their design requirements (Jones, 2006).

The potential structural efficiency of monocoque cylindrical shells in carrying axial loads has been lost due to their extreme sensitivity to geometric imperfections, boundary conditions, loading, etc. and hence for all applications requiring the highest structural efficiency they have been replaced by an alternative structural architecture, the closely stiffened shell, a cylindrical shell reinforced by stringers/corrugations and rings. This alternative architecture is currently established as the premiere efficient aerospace structure (Singer et al., 2002) and is widely used for lightness and extreme efficiency.

We propose an alternative approach that builds on previous work by Ramm and co-workers (Reitinger and Ramm, 1995; Reitinger et al., 1994; Ramm and Wall, 2004), and consists in designing linear-elastic monocoque cylindrical shells with a special cross-sectional shape that maximizes the critical buckling load and at the same time reduces imperfection-sensitivity. These novel shells have asymmetric cross-section and their behavior is fundamentally different from shells designed with the knockdown-factor method.

A key feature of the proposed approach is that the critical buckling loads of both perfect and imperfect candidate designs are introduced in a structural optimization process (Reitinger et al., 1994; Reitinger and Ramm, 1995), and hence its outcome is a design that has a high buckling load and at the same time is also imperfection-insensitive. Standard optimization techniques focus only on maximizing the critical buckling load and tend to converge towards designs that are highly imperfection-sensitive, see for example Thompson (1972). This serious drawback is avoided in the present approach. The optimization technique by Reitinger et al. (1994) and Reitinger and Ramm (1995) is applicable to any

type of structure and hence can also be used to design imperfection-insensitive cylindrical shells with maximal critical buckling loads.

The paper is organized as follows. Section 2 presents the essential background to the present study. It includes: a brief literature review of the influence of imperfections on cylindrical shells; a review of current design approaches to avoid buckling; the selection of appropriate imperfections in buckling analysis; previous work on the design of imperfection-insensitive shells; and structural efficiency metrics for shell buckling. With this background, Section 3 presents a new methodology for the design of imperfection-insensitive cylindrical shells. The implementation in Section 4 produces four designs of carbon-fiber composite cylindrical shells. Section 5 analyzes these results in more detail and Section 6 considers two alternative design approaches. The mass efficiency of the new designs is then compared to existing stiffened shells in Section 7. Section 8 concludes the paper.

2. Background

There is a huge body of literature on the buckling of linear-elastic thin shells and the interested reader is referred to the extensive reviews have been compiled by many authors (Brush and Almroth, 1975; Elishakoff, 2012; Hutchinson and Koiter, 1970; Jones, 2006). This review is focused on the essential background to the present study.

2.1. Effects of Imperfections on Cylindrical Shells

The first major contribution to the present understanding of the effects of initial imperfections on the buckling of circular cylindrical shells was made by Von Kármán and Tsien (1941) who analyzed the postbuckling equilibrium of axially compressed cylindrical shells. Donnell and Wan (1950) analyzed initially imperfect cylindrical shells and obtained equilibrium paths as sketched by the dash line in Fig. 1, where P and P_{cl} are the compressive load and the classical bifurcation buckling load, respectively. Figure 1 shows a sharply dropping second equilibrium path and thus indicates that an initially imperfect shell

buckles at the limit point B instead of reaching the bifurcation point A. Koiter (1963) analyzed the influence of axisymmetric imperfections coinciding with the axisymmetric buckling mode of a perfect cylindrical shell. His results, summarized in Fig. 2, show that imperfections with even a small amplitude can dramatically reduce the buckling load.

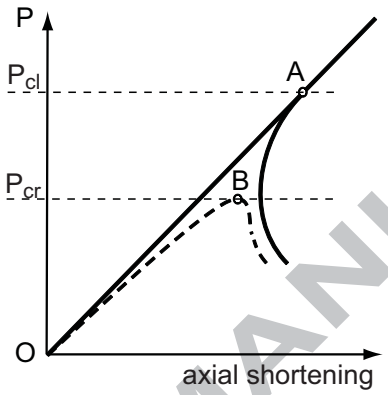

Figure 1: Sketch of equilibrium paths for axially compressed, geometrically perfect cylindrical shells (solid line, from Von Kármán and Tsien (1941)) and imperfect cylindrical shells (dash line, from Donnell and Wan (1950)).

A more general analysis of the influence of initial imperfections (Koiter, 1945) was based on an analysis of the potential energy of the loaded structure in a general buckled equilibrium configuration. This analysis is applicable to asymmetric imperfections and shells of arbitrary shape (Brush and Almroth, 1975), and provides an approximate solution to the secondary equilibrium path for a perfect structure, with a single buckling mode associated with the first bifurcation point:

$$\lambda_0 \equiv \frac{P}{P_{cl}} = 1 + a_1\delta + a_2\delta^2 + ... \tag{1}$$

where $a_1,\ a_2,\ ...$ are constants and δ is a measure of the lateral displacement amplitude. This solution is shown by means of solid lines in Fig. 3. In case I $a_1 \neq 0$ and for small values of δ the secondary equilibrium path is approximated by a straight line. For the other two cases $a_1 = 0$, resulting in quadratic secondary equilibrium paths: $a_2 < 0$ for case II and $a_2 > 0$ for case III.

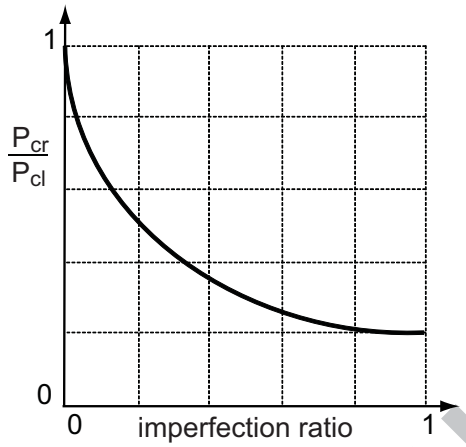

Figure 2: Sketch of influence of imperfection amplitude (ratio of imperfection amplitude to shell thickness) on buckling load P_{cr} of imperfect shells, based on Koiter (1963).

The corresponding equilibrium paths for imperfect structures are shown by dash lines in the figure. $\lambda_{\pm}$ are ratios between the buckling loads of imperfect structures with positive/negative imperfections and the perfect structure. Cases I and II represent structures that are sensitive to imperfections, because the buckling loads of the imperfect structures (λ_{-} for case I and $\lambda_{\pm}$ for case II) are lower than 1. In case I different signs of imperfections lead to different types of imperfection-sensitivity.

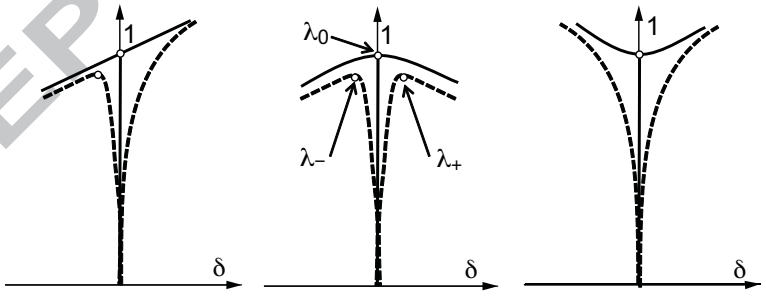

Figure 3: Three types of post-buckling equilibrium paths for perfect and imperfect structures, from Brush and Almroth (1975) and Koiter (1945).

2.2. Design of Cylindrical Shells Against Buckling

The current approach for the design of axially compressed monocoque cylindrical shells against buckling accounts for buckling load reductions due to imperfections through the knockdown-factor method. The actual buckling load of a cylindrical shell is estimated from:

$$P_{cr} = \gamma P_{cl} \tag{2}$$

where γ is the knockdown factor and P_{cl} is given by (Brush and Almroth, 1975):

$$P_{cl} = \frac{2\pi E t^2}{\sqrt{3(1-\nu^2)}} \tag{3}$$

where E, ν and t are the Young's modulus, Poisson's ratio and shell thickness, respectively.

A widely used expression for γ is the empirical curve provided in NASA SP-8007 (Peterson et al., 1965) and shown in Fig. 4. Given the radius to thickness ratio R/t, this curve provides a lower bound to a large dataset of experimentally derived knockdown factors and hence can be used to predict the buckling load using Eq. 2.

Designs obtained from the knockdown factor method are required to achieve a theoretical buckling load P_{cl} high enough that the reduced buckling load P_{cr} obtained from Eq. 2 satisfies the design requirements. Fundamentally, the knockdown-factor design method accepts highly imperfection-sensitive shell designs, but limits the maximum load that can be applied to them, to keep them safe.

An alternative structural form to the imperfection-sensitive monocoque cylinder is the stiffened cylindrical shell. Although it is difficult to make a general comparison, as there are many different potential configurations for the stiffeners, as an example it can be noted that experiments on 12 longitudinally stiffened cylindrical shells with internal or external, integral or Z-stiffeners provided knockdown factors in the range 0.7 to 0.95, indicating a much lower imperfection-sensitivity than monocoque cylindrical shells (Card and Jones, 1966).

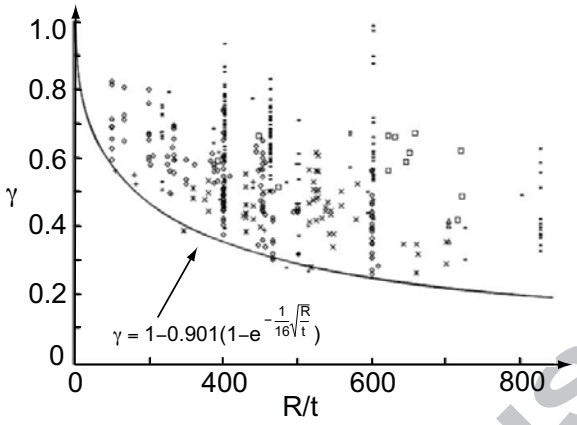

Figure 4: Experimentally measured values of knockdown factor and empirically defined lower bound curve, as a function of the radius to thickness ratio (Jones, 2006).

2.3. Manufacturing Imperfection Signature Approach

The empirically derived lower bound on the knockdown factor in Fig. 4 was derived from many tests conducted over a long period of time and recently it has been argued that the manufacturing, loading and boundary conditions for this large set of shells are not sufficiently well-known to provide a rational basis for modern design. Also, most data points correspond to metallic shells, whereas fiber-reinforced composite shells are not well represented (Jones, 2006; Nemeth and Starnes, 1998). Hence, it has been argued by several authors that the knockdown-factor approach tends to provide overly conservative designs because it allows for the worst possible imperfections which is not a reasonable assumption for modern, precision-made shells.

An emerging alternative design approach is based on the "signature" of the manufacturing imperfection, which is a statistical representation of geometric imperfections based on measurements (Rotter et al., 1992; Teng, 1996; Hilburger and Starnes, 2001; Hilburger et al., 2006; Jones, 2006). This imperfection signature is then applied in the analysis to accurately predict the actual buckling load. Hilburger et al. (2006) obtained the buckling loads of six graphite-epoxy cylindrical shells subject to combined axial compression and

torsion by using five imperfection shapes, including the actual measured imperfections of test specimens, mean imperfection shape, mean imperfection shape plus or minus one standard deviation, and the critical-buckling-mode imperfection shape. The predicted and measured buckling loads of a composite shell with an axially-stiff laminate $[\pm 45/0_2]_s$ are summarized in Fig. 5, where it should be noted that the measured amplitude of imperfection was in the range $+1.27t$ to $-1.54t$.

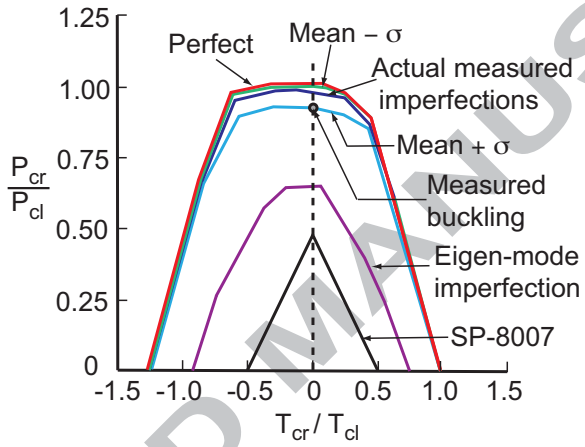

Figure 5: Predicted buckling loads for axially stiff shells under combined axial compression and torsion (Hilburger et al., 2006). P_{cr} and T_{cr} are the axial and torsional buckling loads of imperfect shells; P_{cl} and T_{cl} are the corresponding bifurcation buckling loads of perfect shells; σ is the standard deviation of the imperfection.

Figure 5 shows that the buckling loads predicted using an imperfection based on the critical eigenmode, or using the SP-8007 data(Peterson et al., 1965) are both much lower than the measured buckling load, indicating that using these two approaches can lead to rather conservative designs. Note that the buckling load predicted with the imperfection-signature approach closely matches the measurements.

2.4. Imperfection-Insensitive Shells

Jullien and Araar proposed an intuitive design for imperfection-insensitive cylindrical shells(Jullien and Araar, 1991; Araar, 1990; Araar et al., 1998). Having noted that in a cylindrical shell under axial compression the inward imperfections become amplified whereas the outward imperfections maintain a constant amplitude, these authors considered a cross-sectional shape that is everywhere convex apart from symmetrically distributed, localized kinks. This cross-sectional shape, shown in Fig. 6, is obtained from the critical eigenmode of the shell, by taking the mirror image of all concave arcs. The resulting fluted shell, called the "Aster" shell, is a precursor of the solution proposed in the present paper. A knockdown factor of 0.77 was experimentally demonstrated for an Aster shell with $R = 75$ mm, $t = 153$ μm and a deviation of $+2.3$ mm from the circle.

Figure 6: Cross-sections of dominant eigenmode of circular shell (solid and dashed arcs) and Aster shell (solid line) with $R/t = 490$.

A general shape optimization method for thin shell structures was proposed by Reitinger et al. (1994) and Reitinger and Ramm (1995). Instead of considering only the buckling loads of perfect candidate structures, as in conventional structural optimization, these authors considered both perfect and imperfect structures in the evaluation of the objective function. This fundamental difference avoids convergence towards highly imperfection-sensitive designs.

The method consists of four steps linked in an optimization loop. First, the buckling load of the perfect structure, P_0, and the corresponding eigenmode, Φ,

are computed. Second, the eigenmode is scaled by a prescribed amplitude and is adopted as imperfection shape; it is then superposed to the perfect geometry to define an imperfect shape. Third, the critical buckling load, P_{cr}, for the imperfect structure is calculated. Finally, the minimum among P_0 and P_{cr} is chosen as the value of the objective function.

Applications of this method to the design of concrete shell roofs, stiffened panels and free-form shells were presented by Reitinger and Ramm (1995); Ramm and Wall (2004).

2.5. Efficiency Chart

Quantitative comparisons of different structural designs require the use of suitable metrics. In the present case, the buckling performance of monocoque, stiffened, or any other kinds of cylindrical shells can be compared by considering the weight and load indices (Peterson, 1967; Agarwal and Sobel, 1977; Nemeth and Mikulas, 2009), which are defined as follows:

$$\begin{aligned} &\text{Weight index :} && \frac{W}{AR} \\ &\text{Load index :} && \frac{N_x}{R} \end{aligned} \tag{4}$$

Here W, A, R are the total weight of the shell, the surface area and radius of the cylinder, respectively, and

$$N_x = \frac{P_{cr}}{2\pi R} \tag{5}$$

denotes the (axial) critical buckling stress resultant. The surface area of the shell is $A = 2\pi RL$, where L is the length of the cylinder. Note that the weight and load indices are dimensional, this is the form commonly used by shell designers.

For circular monocoque cylindrical shells, the relation between weight and load indices can be found as follows. Begin by substituting $W = \rho At$ into the weight index expression, which gives

$$\frac{W}{AR} = \frac{\rho t}{R} \tag{6}$$

Then, solve Eq. 3 for t to obtain:

$$t = \sqrt{\frac{P_{cl}\sqrt{3(1-\nu^2)}}{2\pi E}} \tag{7}$$

Then, substitute Eq. 7 into Eq. 6 and replace P_{cr}/γ for P_{cl}, from Eq. 2, to obtain:

$$\frac{W}{AR} = \frac{\rho}{R}\sqrt{\frac{P_{cr}\sqrt{3(1-\nu^2)}}{2\gamma\pi E}} \tag{8}$$

Further substitution of $2\pi R N_x$ for P_{cr} , from Eq. 5, and simplification gives:

$$\frac{W}{AR} = \rho\sqrt{\frac{\sqrt{3(1-\nu^2)}}{\gamma E}\frac{N_x}{R}} \tag{9}$$

Figure 7 shows a plot of W/AR vs. N_x/R. The inclined straight line in the figure represents perfect ($\gamma = 1$) monocoque aluminum shells; the horizontal line corresponds to lightly-loaded shells which are subject to a minimum thickness constraint. The data points included in the plot represent; (a) shells with integral-orthogonal stiffeners under axial compression (Katz, 1965); (b) z- and integrally-longitudinally stiffened shells under axial compression (Card, 1964a); (c) a corrugated graphite-epoxy ring-stiffened cylinder under bending (Davis, 1982); (d) ring-stiffened corrugated cylinders under axial compression (Peterson, 1967); and (e) z-stiffened shells subject to bending (Card, 1964b). Note that for structures subjected to bending the critical axial stress resultant used in the calculation of the load index was the peak axial stress resultant due to the critical bending moment, obtained from simple bending theory.

Shells closer to the right-bottom corner of the chart are the most efficient, as they can carry larger loads using less material. The chart shows that most stiffened cylindrical shells have higher efficiency than even perfect monocoque circular cylindrical shells. However, it should be noted that the reduced imperfection-sensitivity of stiffened cylindrical shells is countered by their complex manufacturing process. Machining from thicker stock and special forgings are the main manufacturing methods for metallic shells (Singer et al., 2002). In 1986 the cost of a 320 mm diameter steel shell stiffened in one direction was on the order of

$3,500, and of $15,000 for a similar, orthogonally stiffened shell (Scott et al., 1987; Singer et al., 2002).

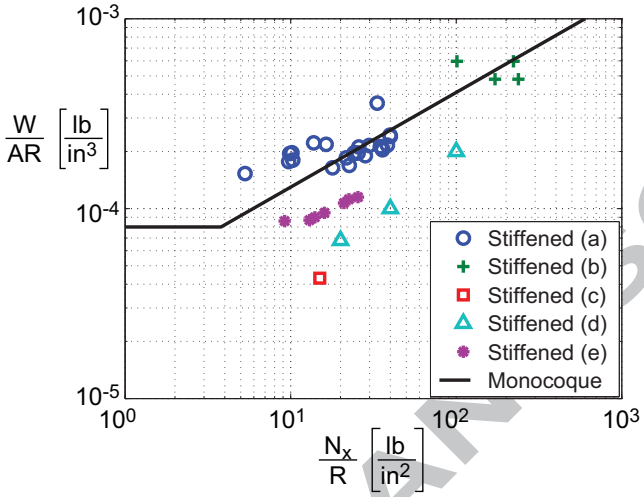

Figure 7: Performance chart for stiffened cylindrical shells described in Section 2.5 (data provided by Dr. M.M. Mikulas) and including plot of Eq. 9 for perfect ($\gamma = 1$) monocoque cylinders.

3. Methodology

We have adopted the method of Ramm and co-workers (Reitinger et al., 1994) to search for the cross-sectional shape of imperfection-insensitive monocoque linear-elastic cylindrical shells with maximal buckling load. This section presents the methodology to parameterize the shape of the cross-section and to formulate the design problem; the implementation of the design process is also presented.

3.1. Parametrization of Cross-Section

The improved buckling load and decreased sensitivity to imperfections of the Aster shell motivated us to explore corrugated shells with general cross-sectional shapes and to introduce the concept of the wavy shell, shown in Fig. 8.

The cross-section of the wavy shell is defined by a set of control points, with a NURBS (Non-Uniform Rational B-Spline) interpolation creating a smooth curve through the control points. The NURBS is given by (Hughes et al., 2009):

$$C(\xi) = \sum_{i=1}^{n} N_{i,p}(\xi) B_i, \tag{10}$$

where $N_{i,p}$ is a piecewise base function and B_i is a vector of control points. ξ, p and n denote a parametric coordinate, the order of NURBS and the number of base functions, respectively. The base functions are recursively defined as (Hughes et al., 2009):

$$N_{i,p}(\xi) = \frac{\xi - \xi_i}{\xi_{i+p} - \xi_i} N_{i,p-1}(\xi) + \frac{\xi_{i+p+1} - \xi}{\xi_{i+p+1} - \xi_{i+1}} N_{i+1,p-1}(\xi). \tag{11}$$

For $p = 0$:

$$N_{i,0}(\xi) = \begin{cases} 1 & \text{if } \xi_i \leq \xi \leq \xi_{i+1}, \\ 0 & \text{otherwise} \end{cases} \tag{12}$$

where ξ_i is the i^{th} knot in the knot vector $\Xi = (\xi_1,\ \xi_2,\ ..., \xi_{n+p+1})$. In the present study, 3^{rd} degree NURBS with uniform knots, i.e. $\Xi = (1,\ 2,\ ...,\ n+4)$, were chosen. These base functions are periodic, which guarantees that the closed cross-section generated by this NURBS has smooth slope and curvature everywhere.

The wavy shell is defined to be axially uniform, so that the longitudinal stress resultant is the dominant one. A varying cross-section would induce shear and possibly even bending when the shell is loaded under axial compression, resulting in a decrease in the axial stiffness of the shell and its buckling load.

Two main geometric constraints were introduced to narrow down the design space. First, the control points were defined to be circumferentially equally spaced and radially within a distance Δr from a reference circle of radius R, see Fig. 8. This radial limit avoids excessive curvature of the wavy cross-section. The circumferential position of the i^{th} control point in the first quadrant, $\theta_{1,i}$, is given by:

$$\theta_{1,i} = \frac{\pi(i-1)}{2(N-1)}, \tag{13}$$

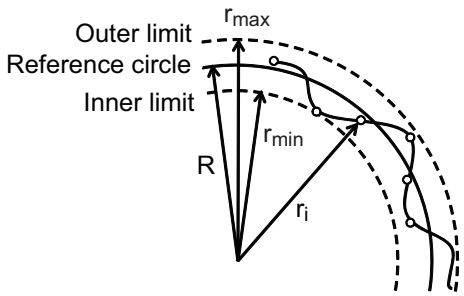

Figure 8: Definition of wavy shell geometry showing also several control points.

where N is the total number of control points in the first quadrant, including any control points lying on the x- and y-semi-axes.

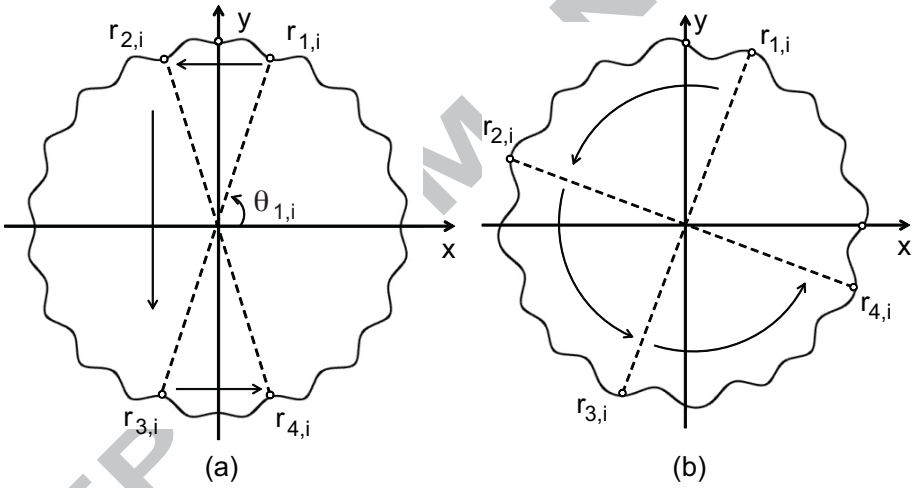

Figure 9: Cross sections with (a) mirror-symmetry and (b) 4-fold symmetry. $r_{q,i}$ denotes the radial position of the i^{th} control point in the q^{th} quadrant.

Second, to further narrow down the design space, the wavy section was assumed to be either mirror-symmetric with respect to the x- and y-axes, as shown in Fig. 9 (a), or 4-fold rotationally symmetric as shown in Fig. 9 (b). In the first case there are only N control points in the first quadrant (of which two lie on the x and y-axes) that divide it into $N-1$ sectors subtending equal angles. In the second case only $N-1$ control points are needed (of which one

lies on the axis) and all other points are obtained by rotation operations. Note that the two symmetry schemes with N and $N-1$ control points result in the same spatial resolution for the wavy cross-section.

Thus, the cross-section is defined by:

$$C = \begin{cases} C(r_{1,1},\ r_{1,2},\ ...,\ r_{1,N}) & \text{mirror-symmetry,} \\ C(r_{1,1},\ r_{1,2},\ ...,\ r_{1,N-1}) & \text{4-fold symmetry} \end{cases} \tag{14}$$

3.2. Formulation of Optimization Problem

For every candidate cross section, C, the objective function is defined as the minimum among the following three buckling loads:

- the bifurcation buckling load, P_0, of the geometrically perfect structure;
- the buckling load, P_+, of a geometrically imperfect structure obtained by superposing an imperfection of positive sign onto the perfect structure; and
- the buckling load, P_-, of a structure with an imperfection of negative sign.

The imperfection shape was chosen as the first (critical) buckling mode, for the following reasons. First, finding the actual imperfection shape that leads to the lowest buckling load is, after many years of research, still an open issue; a widely used approach is to use the critical buckling mode, see for example Ramm and Wall (2004), Hilburger et al. (2006) and Jones (2006). Second, tests and analyses carried out by Hilburger et al. (2006) and reviewed in Section 2.3 have shown that the critical-mode imperfection leads to lower buckling load predictions than the actual values, indicating that it is a conservative choice that provides a lower bound on the buckling loads that can be expected in practice. Third, we have carried out a detailed optimization study of wavy cylinders in which the first four critical modes were used to define the imperfection shape. Compared with the designs obtained using only the first critical mode, the reduction in the buckling loads with the additional imperfections was only 3%. In conclusion, the critical buckling mode is adequate for the present study.

Figure 10 shows the geometrically perfect structure and one of the two imperfect structures that were analyzed at one step of the optimization process.

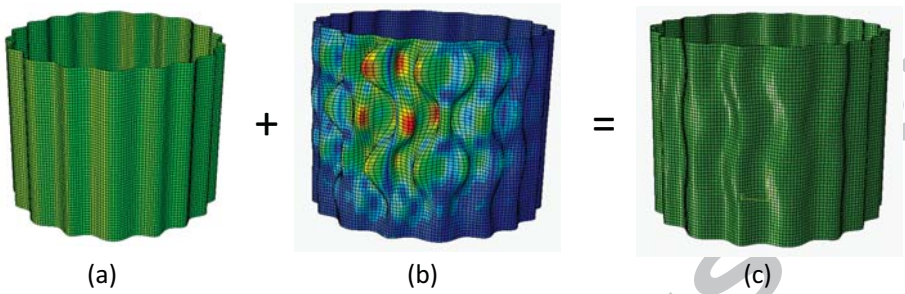

Figure 10: (a) Wavy shell with perfect geometry, $C_0(r_{1,1},\ r_{1,2},\ ...)$; (b) imperfection shape based on critical buckling mode, $\mu\Phi$, with $\mu = 10t$ for clarity; (c) imperfect wavy shell, $C_+ = C_0(r_{1,1},\ r_{1,2},\ ...) + \mu\Phi$.

The imperfection amplitude was set equal to the shell thickness. According to Fig. 2 this amplitude will cause a five-fold decrease in the buckling load and hence provides a significant challenge for the present search for imperfection-insensitive designs. Of course, the actual amplitude of the imperfections depends on the manufacturing processes that are adopted; the effects of imperfection amplitudes larger than t is analyzed in Section 5.3.

Regarding the sign of the imperfections, both positive and negative imperfection signs need to be considered in order to capture the different types of imperfection-sensitivity discussed in Section 2.1.

In summary, the optimization problem was formulated as follows:

$$\begin{aligned}
&\text{Maximize :} \quad \min\,(P_0, P_+, P_-)\\
&\text{among all wavy shells with either mirror-symmetric or 4-fold symmetric}\\
&\text{cross-sections, defined by the control variables:}\\
&r_{1,i},\ i = 1,\ 2,\ 3,\ ...\\
&\text{that are subject to :}\\
&|r_{1,i} - R| \ \leq\ \Delta r,\ i = 1,\ 2,\ 3,\ ....
\end{aligned} \tag{15}$$

where:

- P_0, P_+, and P_- are respectively the buckling loads of wavy shells with perfect geometry, imperfect geometry with positive imperfection, and imperfect geometry with negative imperfection;
- the positive imperfection is $+t\Phi$ and the negative imperfection is $-t\Phi$.

3.3. Numerical Implementation

Our implementation of the design optimization problem was based on existing software, including commercial computer-aided design (CAD) and finite-element analysis (FEA) software, and an open-source optimizer, all run by a Matlab script. This section describes the three softwares that were used and how they were interfaced.

The NURBS-based CAD software Rhino 3D (version 5.0) was used to create CAD models of the cross-sections of the perfect wavy shells. The NURBS interpolation solver embedded in Rhino 3D was used to read a text file containing the positions of the control points and to create the cross-section geometry, which was then exported as an Initial Graphics Exchange Specification (.IGS) file. This process was automated by means of a Python script.

The optimization process requires FEA software that can be automated through a scripting interface to set up analysis models and run non-linear buckling analyses. There exists some very efficient finite element formulations for axisymmetric shells, such as shell elements based on Fourier analysis for the buckling analysis of cooling towers (Combescure and Pernette, 1989). This formulation can also be used to analyze the influence of Fourier mode imperfections on the non-linear buckling behavior of an axisymmetric shell, however it is not applicable to the present situation.

The general purpose package Abaqus 6.11 was chosen. Abaqus/CAE was used to read the .IGS file, set up three structural models (the first model with the perfect geometry and the two others with imperfect geometries based on either positive or negative imperfections), and compute the buckling load for each model. For each candidate design, a Python script set up an Abaqus/Standard

model including about 20,000 fully-integrated quadrilateral thin-shell elements (element S4) of the shell with perfect geometry. A linear eigenvalue buckling analysis was carried out on this initial model to compute the critical eigenmode, Φ. Next, the displacements of the nodes according to the first eigenmode were extracted from the Abaqus/Standard output file and were scaled with the maximum transverse displacement equal to the shell thickness.

Two FEA models of imperfect shells were obtained by superposing the scaled displacements on the mesh of the perfect shell. For the perfect geometry and also for each of the imperfect geometries, the critical buckling load was computed by carrying out a load-displacement arc-length incrementation non-linear analysis, using the Riks solver in Abaqus/Standard.

Figure 11 shows plots of the relationship between axial load vs. axial displacement, obtained from non-linear analyses of the perfect shell and both imperfect shells. In each load-displacement curve, the first limit load has been taken as the buckling load. The Abaqus/Standard Riks solver may turn back at the first limit load and fail to compute the post-buckling behavior. This was not an issue in the present case, since only the buckling load value is of interest. The increments in the arc-length were automatically determined by the solver, and the first limit loads were usually reached after 10 to 30 increments. The maximum number of increments was set to 50, which was sufficient to reach the first limit load in all examples presented in this paper.

The results of our simulations were checked by changing the maximum allowed increments from a large value (typically, 1 kN) down to a small value (100 N); the differences between these two cases were found to be within 1%. It should be noted that Abaqus automatically reduce the increment as the non-linearity of the response increases. It was found that a typical increment was less than 5 N when the applied loads are close to the bifurcation points.

Lastly, the Evolution Strategy with Covariance Matrix Adaption (CMA-ES)(Hansen et al., 2003) and Hansen (2011) open source algorithm (Hansen, 2012) was used as the optimizer. The background to this choice is that the optimization problem in Eq. 15 does not have an explicit mathematical expres-

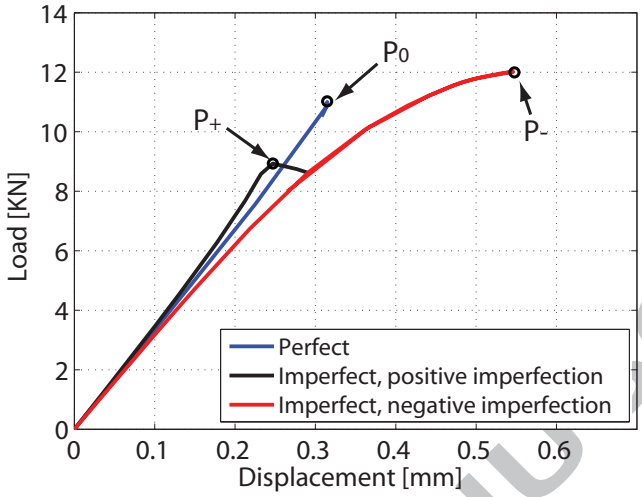

Figure 11: Schematic of equilibrium diagrams for geometrically perfect and imperfect shells, showing definition of limit loads. In the example shown the load-displacement curves for the perfect shell and the imperfect shell with negative imperfection turn back at the first limit load.

sion and, due to the highly non-linear relationship between shape and buckling loads, the objective function is expected to be non-convex. Therefore, evolutionary optimizers were evaluated and CMA-ES was selected for its efficiency, see Bäck (1996) for a review of basic concepts.

An initial population of eight wavy shells was randomly chosen. Shells with higher $min(P_0, P_+, P_-)$ were ranked higher. The top 4 designs in the population of each generation were selected as parents and their design variables were recombined and mutated to create 8 offspring structures for the next generation. The critical loads, P_0, P_+, and P_-, of the best design in each generation were recorded. After running the optimization for a set number of iterations, typically 150, the structure with maximal $min(P_0, P_+, P_-)$ was taken as the final solution.

The simulations were run on a Xeon X5680 server with 12 CPUs on a single motherboard. Tests showed that simultaneously running 4 jobs on 3 CPUs for each job minimized the average simulation time. A population size that

is a multiple of 4 can best use this computational resource and, due to the small number of design variables considered in the present study, the population size was chosen as 8. The total simulation time to evaluate (P_0, P_+, P_-) for a population of 8 structures was about 1 hour.

4. Wavy Shell Designs

Four imperfection-insensitive carbon-fiber composite shells with a common set of dimensions and material properties, loaded under axial compression and clamped at both ends are presented.

4.1. Dimensions and Material Properties

The shells were chosen to have a square aspect ratio, which is a common choice for studies of shell buckling, see for example Arbocz and Babcock (1968), Davis (1982) and Hilburger et al. (2006). The dimensions presented in Table 1 were chosen, for practical considerations that will be addressed in a follow-on paper on experimental testing,

Table 1: Dimensions of wavy shell designs

Thickness, t	180 μm
Radius, R	35 mm
Length L	70 mm
Maximum deviation from circle, Δr	1.5 mm

A symmetric six-ply laminate, $[+60°, -60°, 0°]_s$ was adopted, where the 0° direction of the laminate is in the axial direction of the shell. It consisted of 30 μm thick unidirectional laminae of T800 carbon fibers and ThinPreg 120EPHTg-402 epoxy, provided by the North Thin Ply Technology company, with a fiber volume fraction of approximately 50%. The following lamina properties were measured: $E_1 = 127.9$ GPa, $E_2 = 6.49$ GPa, $G_{12} = 7.62$ GPa, and $\nu_{12} = 0.354$, where E_1 is the modulus along the fiber direction. The ABD matrix of the

laminate was calculated from these properties, using classical lamination theory (Daniel and Ishai, 2006):

$$ABD = \begin{pmatrix} 9.919 \times 10^6 & 2.670 \times 10^6 & 0 & 0 & 0 & 0 \\ 2.670 \times 10^6 & 9.919 \times 10^6 & 0 & 0 & 0 & 0 \\ 0 & 0 & 3.625 \times 10^6 & 0 & 0 & 0 \\ 0 & 0 & 0 & 0.0108 & 0.0099 & 0.0034 \\ 0 & 0 & 0 & 0.0099 & 0.0373 & 0.0081 \\ 0 & 0 & 0 & 0.0034 & 0.0081 & 0.0125 \end{pmatrix} \tag{16}$$

where the units of the A and D matrices are N/m and Nm, respectively.

4.2. Reference Cylindrical Shell

A buckling analysis of a reference circular shell, made from the laminate selected in Section 4.1 and with the geometric properties defined in Table 1, was carried out. The assumed geometric imperfection was based on the critical buckling mode, shown in Fig. 12, with amplitude $\mu = t$. The buckling loads were 4.153, 1.137, and 1.137 kN, respectively for the geometrically perfect shell and the shell with positive and negative imperfections.

The knockdown factor is calculated from:

$$\gamma = \frac{\min(P_+, P_-)}{P_0} \tag{17}$$

which gives 0.274. The critical stress is calculated from:

$$\sigma_{cr} = \frac{\min(P_0, P_+, P_-)}{l_p t}, \tag{18}$$

where l_p and t are the arclength of the (wavy) center line and the thickness of the shell. Its value is 28.724 MPa.

4.3. Mirror-Symmetric Shells

Two mirror-symmetric wavy shells with $N = 11, 16$ were designed. The optimization was first run for the case $N = 16$ and, since this initial run had

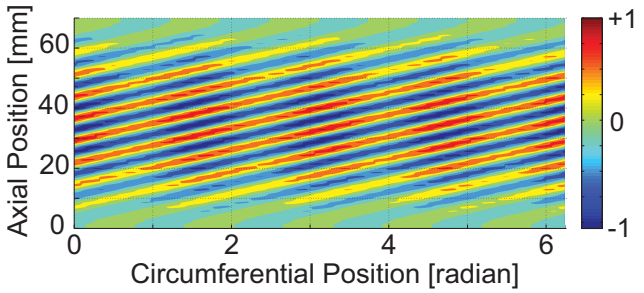

Figure 12: Critical buckling mode of reference (circular) cylindrical shell.

converged long before the 150th generation, all other optimizations were also run for 150 generations. The evolution of the buckling loads (divided by the buckling load of the perfect, reference cylindrical shell) for the perfect and imperfect candidate designs for these two cases is shown in Fig. 13. An optimum design for the case $N = 11$ occurred at the 66th generation, with buckling loads of 11.017, 10.145 and 11.420 kN, respectively for the perfect shell and the imperfect shells with positive and negative imperfections. The optimum for the case $N = 16$ occurred at the 126th generation, with buckling loads of 14.981, 14.908 and 14.897 kN, respectively.

Note that in Fig. 13(a) P_- is almost always larger than P_0 which is in turn larger than P_+, suggesting that the majority of candidate designs considered during this optimization behave according to Case I in Fig. 3. Also note in the enlargement of Fig. 13(b) that after the 37th generation the candidate designs have slightly lower buckling loads for the imperfect cases than for the perfect shell, indicating that in this case the candidate designs behave according to Case II.

The cross-sections obtained for the two cases are shown in Fig. 14, and the optimal radial positions of the control points are presented in Table 2.

The knockdown factor is calculated from Eq. 17, which gives 0.921 and 0.994 for the cases $N = 11, 16$, respectively. The critical stress is calculated from Eq. 18 which gives 224.639 and 310.494 MPa, respectively for $N = 11, 16$.

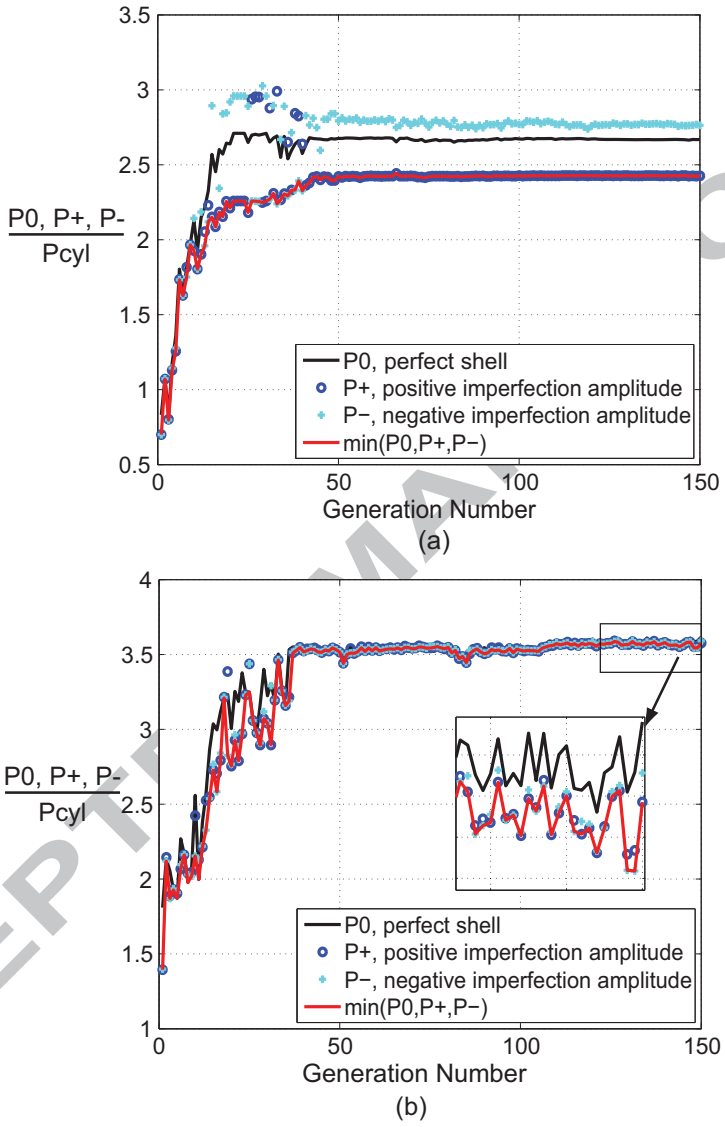

Figure 13: Evolution of buckling loads for mirror-symmetric wavy shells with (a) $N = 11$ and (b) $N = 16$. The loads are normalized by the buckling load of the perfect, reference cylindrical shell.

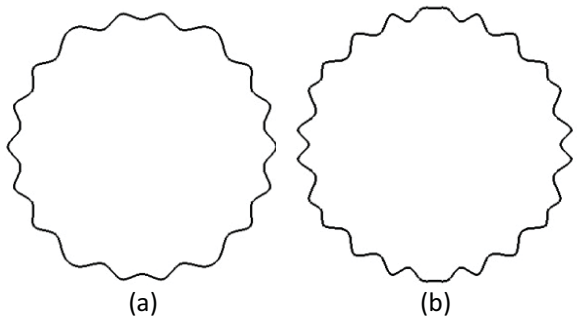

Figure 14: Cross-sections of mirror-symmetric wavy shells with (a) $N = 11$ and (b) $N = 16$.

Table 2: Radial deviations, $r_i - R$, (in mm) of control points of mirror-symmetric shells.

Point	1	2	3	4	5	6	7	8	9	10	11	12	13	14	15	16
N=11	1.5	-1.5	1.5	-1.5	1.5	-1.5	1.5	1.5	-1.5	1.5	0					
N=16	-1.5	1.5	-1.5	-1.5	1.5	0	1.5	-1.5	-1.5	1.4	-1.5	-1.2	1.5	-1.5	1.1	1.4

4.4. 4-Fold Symmetric Shells

4-fold symmetric wavy shells were also designed. These designs are also denoted as $N = 11, 16$, although the actual numbers of independent control points used in the optimization were in fact $10, 15$, respectively, as explained in Section 3.1.

The evolution of the buckling loads is plotted in Fig. 15 where it can be seen that both cases converge to the Case II buckling. The best design for the case $N = 11$ was obtained at the 49th generation, with buckling loads of 10.587, 9.325 and 9.310 kN for the perfect shell and for imperfect shells with positive and negative imperfections, respectively. The best design for the case $N = 16$ was obtained at the 127th generation, with buckling loads of 13.609, 13.534 and 13.536 kN, respectively. The knockdown factors for the two cases were 0.879 and 0.994 and the corresponding critical stresses 208.224 and 281.712 MPa.

Figure 16 shows the cross-sections of the two 4-fold symmetric cross-sections obtained from this study. The optimal radial deviations of the control points from the reference circle are presented in Table 3.

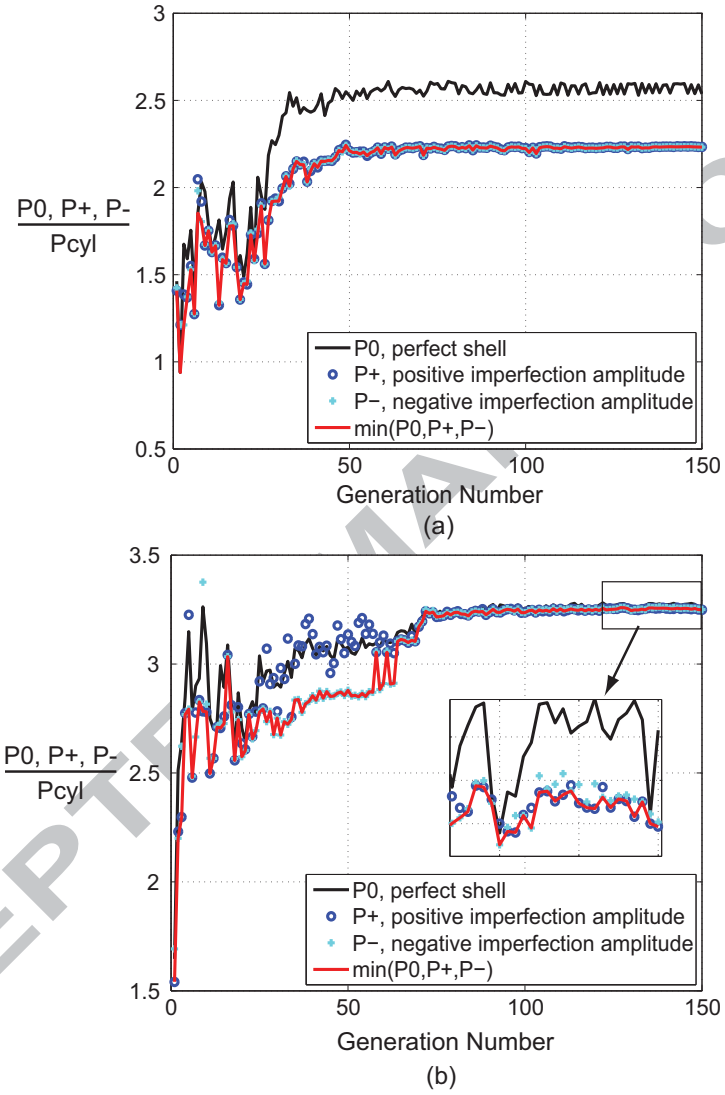

Figure 15: Evolution of buckling loads for 4-fold symmetric wavy shells with (a) $N = 11$ and (b) $N = 16$. For the case $N = 16$ $P_{\pm}$ is slightly lower than P_0 after the 72nd generation. The loads are normalized by the buckling load of the perfect, reference cylindrical shell.

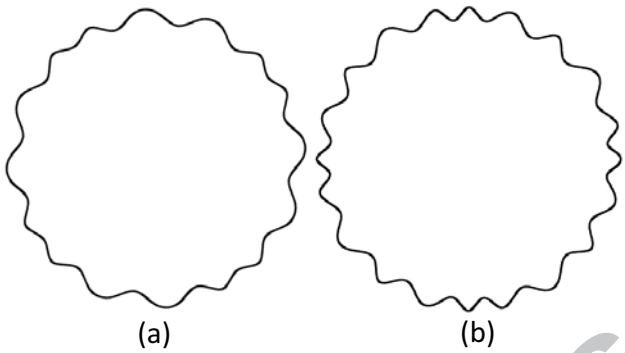

Figure 16: Cross-sections of 4-fold symmetric wavy shells with (a) $N = 11$ and (b) $N = 16$.

Table 3: Radial deviations of control points, $r_i - R$, (in mm) of 4-fold symmetric shells.

Point	1	2	3	4	5	6	7	8	9	10	11	12	13	14	15	16
N=11	1.5	1.5	-1.5	1.5	0	1.5	-1.5	1.5	1.3	-1.5	1.5					
N=16	1.5	-1.5	1.5	0	-1.5	1.4	1.5	-1.5	-1.5	1.4	-1.5	-1.5	1.5	0	-1.5	1.5

5. Comparison and Analysis of Wavy Shell Designs

Starting with a comparison of the predicted performance of the four shell designs obtained in the previous section, a deeper insight into the proposed approach is then obtained by considering the component wavelengths of each design. Also, an analysis of the effects of increasing the amplitude of imperfections in wavy cylinders confirms the robustness of the present approach.

5.1. Comparison

The knockdown factor and the critical stress for each wavy shell design presented in Sections 4.3-4.4, calculated from Eqs. 17-18, are presented in Table 4.

Note that the knockdown factor and the critical stress of the mirror-symmetric shell with $N = 16$ are respectively 7.9% and 38.2% higher than for the shell with $N = 11$ and the same type of symmetry; for 4-fold symmetric shells, these values increase respectively by 13.1% and 35.3% when N is increased from 11 to 16. These results show that increasing the number of control points leads

Table 4: Length of center line, knockdown factor and critical stress for 180 μm thick carbon-fiber composite shells with reference radius of 35 mm.

Symmetry	N	l_p [mm]	γ	σ_{cr} [MPa]
Mirror	11	250.897	0.921	224.639
	16	266.547	0.994	310.494
4-Fold	11	248.373	0.879	208.244
	16	266.900	0.994	281.712
Circular	N/A	219.911	0.274	28.724

to decreased imperfection-sensitivity and improved critical stresses. Compared with mirror-symmetric wavy shells, 4-fold symmetric wavy shells have lower critical stresses and smaller or equal knockdown factors, suggesting that mirror symmetry is a better choice.

Compared to the reference circular shell presented in Section 4.2, the critical stress of the best wavy shell design ($N = 16$ and mirror-symmetric) is 981% higher and the knockdown factor is 263% higher. This result indicates that the introduction of wavy cross-sections has dramatically reduced imperfection-sensitivity, and the critical stress has also been significantly improved.

5.2. Analysis of Shell Cross-Sections

A better understanding of the wavy shell designs generated in Sections 4.3-4.4 can be obtained by decomposing each cross-section profile into a series of periodic waveforms. We used the Fast Fourier Transform function in Matlab to compute these components, to obtain the coefficients of the decomposition:

$$A(k) = \sum_{n=0}^{m-1} a_n e^{-i2\pi k \frac{n}{m}},\ k = 0, 1,\ 2,\ ...,\ m-1 \tag{19}$$

where k is the wave number and m is the number of sampling points, chosen as 1000. a_n is the radial deviation of the n^{th} sample point from the reference circle:

$$a_n = r_n - R. \tag{20}$$

The results are plotted in Figs 17-18, for the range $k = 0, 1, \ldots, 49$.

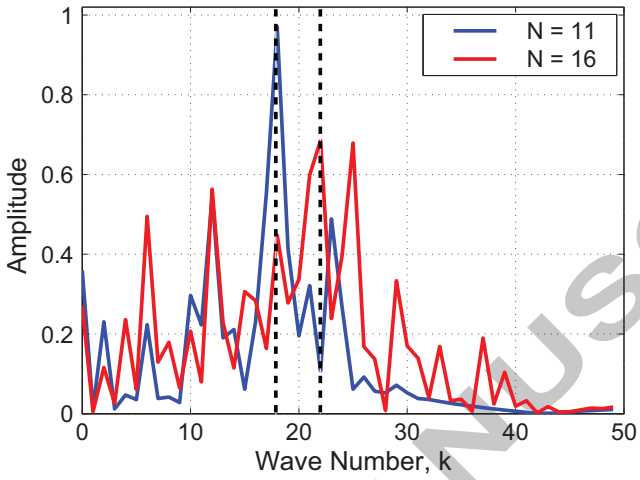

Figure 17: Components of mirror-symmetric wavy shells.

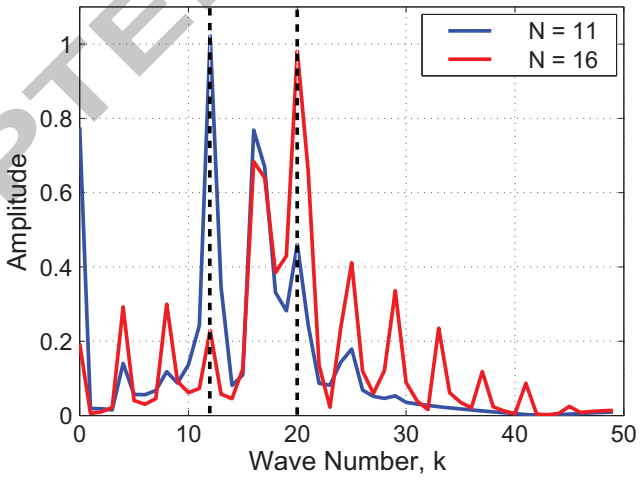

Figure 18: Components of 4-fold symmetric wavy shells.

Comparisons between different designs can be made more easily if we define the peak wave number, equal to the wave number k corresponding to the maximum amplitude $A(k)$, and the bandwidth of the distribution. equal to the maximum wave number whose amplitude is no less than 10% of the amplitude of the peak component. It can be noted in Figs 17-18 that both the peak wave number and the bandwidth increase as the number of control points is increased from $N = 11$ to $N = 16$.

The peak wave number and the bandwidth of all wavy shells obtained in the present study are presented in Table 5. These results, along with the knockdown factors and the critical stresses in Table 4, indicate that higher peak wave numbers and wider bandwidths tend to lead to higher critical stresses and knockdown factors. The spatial component distributions for each particular type of symmetry show that the shell designs with the largest knockdown factor and critical stress tend to have several components with large amplitudes rather than a single peak, suggesting that an optimal combination of several different components is desirable.

Table 5: Peak wave number and bandwidth of wavy cylinder designs.

Symmetry	N	Peak Wave Number	Bandwidth
Mirror	11	18	23
	16	22	39
4-Fold	11	12	25
	16	20	37

5.3. Effects of Imperfection Amplitude

In the previous optimization study the amplitude of the imperfections was assumed to be equal to one shell thickness. Because there are many factors that affect this parameter (Singer et al., 2002), and even recent studies (Hilburger et al., 2006) have reported imperfections larger than t, it is desirable to study the effects of a range of imperfection amplitudes.

Instead of re-running the optimization study with different imperfection amplitudes, we took the wavy shell geometries obtained in Section 4, superposed the critical-buckling-mode imperfection with amplitudes of $\pm 0.5t$, $\pm 2t$ on the perfect geometry, and calculated the corresponding buckling loads, $P_{\pm}$, using the Riks solver in Abaqus/Standard. Equation 17 was then applied to calculate the knockdown factors for these shells and the results are presented in Table 6. The general data shown by the data is that the knockdown factor decreases when μ increases. The reduction is largest for the mirror-symmetric shell with $N = 11$ for which the knockdown factor decreases by 11.13% for μ increasing from $0.5t$ to $2t$, so this particular design is rather sensitive to the imperfection amplitude. However, for the other three designs the reduction is quite small. In particular, note that both designs with $N = 16$ show a reduction of only 2% for μ increasing from $0.5t$ to $2t$.

Table 6: Sensitivity of knockdown factors to imperfection amplitude.

Symmetry	N	$\mu = 0.5t$	$\mu = t$	$\mu = 2t$	Overall Reduction %
Mirror	11	0.952	0.921	0.846	11.13
	16	0.999	0.994	0.979	2.00
4-Fold	11	0.908	0.879	0.854	5.95
	16	0.997	0.994	0.977	2.01

6. Comparison to Alternative Shell Designs

Here we compare the symmetry-breaking cross-section designs obtained in Section 4 with alternative designs, based either on a sinusoidally corrugated shape or on the fluted shape of the Aster shell.

6.1. Sinusoidally Corrugated Shells

Shells with a periodic cross-section were obtained by superposing a sinusoidal wave on the reference circle:

$$r(\theta) = R + \Delta r \sin(k\theta), \tag{21}$$

where k is the total number of waves and Δr their amplitude. The dimensions and material properties of the shell were unchanged from Section 4.

The buckling loads of sinusoidally corrugated shells with three different amplitudes of the corrugation, Δr, and a perfect geometry are plotted in Fig. 19. The trend is that the buckling load increases as the wave amplitude increases beyond a transition number of waves, k, and the transition occurs at smaller values of k for larger Δr's.

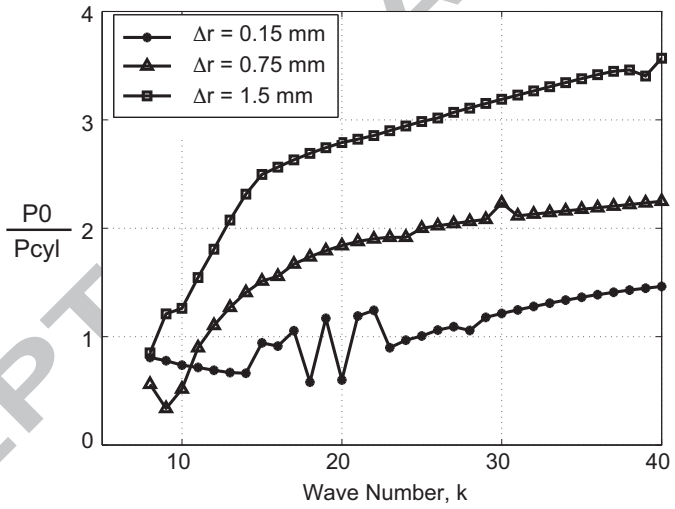

Figure 19: Buckling loads of geometrically perfect sinusoidally corrugated shells with corrugations of three different amplitudes.

Both perfect and imperfect sinusoidally corrugated shells were also analyzed for the case $\Delta r = 1.5$ mm, which coincides with the maximum deviation from the reference circle allowed in Section 4. As in Section 4, the geometry of the imperfect shells was obtained by superposing the scaled critical buckling mode

on the perfect geometry:

$$C_{\pm}(k) = C_0(k) \pm \mu\Phi, \tag{22}$$

where $C_0(k)$ and $C_{\pm}(k)$ are the shapes of the perfect and imperfect shells, respectively; Φ is the critical eigenmode obtained from a linear eigenvalue analysis, and the amplitude of the imperfection $\mu = t$. The buckling loads of the perfect and imperfect shells, P_0 and $P_{\pm}$, were obtained, as before, from non-linear arc-length controlled simulations, for sinusoidal shells with $k = 8, \ldots, 40$.

Then the knockdown factor and the critical stress for each value of k were calculated from Eqs 17-18; their values are plotted in Fig. 20. The plot of knockdown factors, Fig. 20(a), shows an initial region of rapid increase as k increases from 8 to ≈ 10, followed by a dip and a region of much less rapid increase for $k > 15$. The plot of critical stress, Fig. 20(b), shows a rapid increase in the range $k = (8, 15)$, followed by an asymptotic increase toward 220 MPa. Together, these plots indicate that, for the specific case $R = 35$ mm that is being considered, sinusoidally corrugated shells with around 10 corrugations are effective in decreasing the imperfection sensitivity, however there is a diminishing return for further increasing the number of corrugations. In fact, it will be seen in Section 7 that the mass efficiency actually begins to slightly decrease beyond $k \approx 15$.

The knockdown factor and the critical stress of the wavy shells in Section 4 are also plotted in Fig. 20, using in each case the peak wave number as the characteristic value of k. These plots show that the wavy shell designs are significantly more effective in increasing both values. However, it should be noted that the sinusoidal shells require only two design variables (wave number and amplitude), leading to simpler designs and potential simplification in manufacturing than the proposed wavy shells. Figure 20(b) shows a significant increase in the critical stress as the number of control points is increased from 11 to 16. It would be interesting to further explore this trend and establish at what value of N a limit may be reached.

A comparison of the critical buckling modes of the different shell designs that

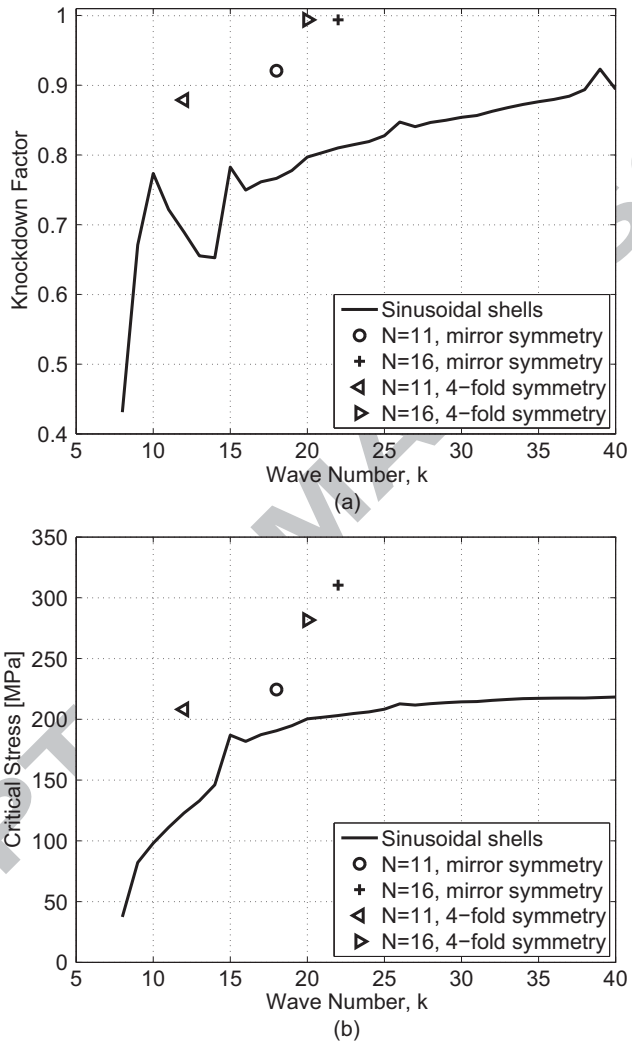

Figure 20: Comparison of (a) knockdown factor and (b) critical stress of sinusoidally-corrugated shells and wavy shell designs obtained in Sections 4.3-4.4.

have been considered provides further insights. At $k = 15$ the critical mode of sinusoidally corrugated shells switches from a helical sequence of inward and outward dimples, Fig. 21(a), to much larger, circumferentially arranged inward dimples with axial wavelength equal to the length of the shell, Fig. 21(b). This switch marks the change in behavior that has been highlighted by the two different trends seen in Fig. 20.

Figure 22 shows the critical buckling mode of the mirror-symmetric wavy shell with $N = 16$. In this case the mode is localized along a narrow axial strip.

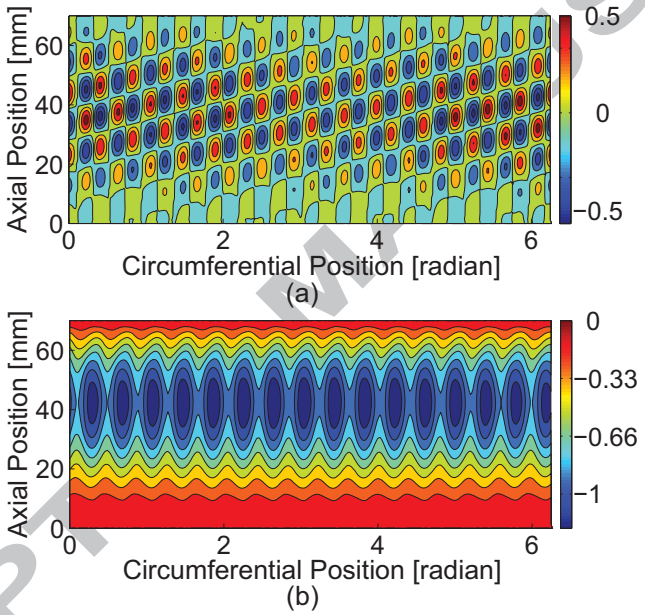

Figure 21: Typical critical buckling modes of sinusoidally corrugated shells with (a) $k \leq 15$ and (b) $k > 15$.

These results suggest that the optimized behavior achieved in our best designs is related to the symmetry-breaking feature of the wavy cross-sections, which delays the transition of local buckling modes into global modes.

6.2. Aster Shell

The Aster shell, described in Section 2.4, was the first imperfection-insensitive corrugated shell design to be tested experimentally. Jullien and Araar (1991)

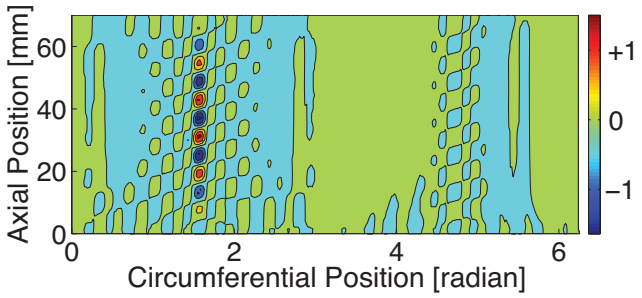

Figure 22: Critical buckling mode of mirror-symmetric wavy shell with $N = 16$.

designed, built and tested a nickel shell with 22 corrugations and radius, length, and thickness given by R=75 mm, L=120 mm and t=153 μm. A reference circular cylindrical shell with thickness of 150 μm was also built and tested. The values of the modulus and Poisson's ratio of these nickel shells, provided in Araar (1990), are $E = 162$ GPa, $\nu = 0.3$. Both shells were clamped at the ends and tested under axial compression; the measured buckling loads were 14.2 kN and 11.0 kN, respectively for the Aster shell and the circular shell.

A study of the buckling loads of both structures was carried out using the same approach used throughout this paper, namely an imperfection based on the critical buckling mode scaled to an amplitude of one thickness was applied in a geometrically non-linear, arc-length controlled simulation to estimate the limit load. In this way, estimates were obtained for the buckling loads of the geometrically perfect structures, and also for imperfect structures with imperfections of both positive and negative signs. The resulting sets of values were 18.328, 16.405, and 16.418 kN for the Aster shell and 14.606, 5.295, and 5.294 kN for the circular cylinder; these values were used to estimate the theoretical knockdown factor from Eq. 17 and the theoretical critical stress from Eq. 18. The values obtained in this way are presented in Table 7.

A competing wavy cylinder design with a mirror-symmetric cross-section with $N = 11$ control points was obtained, considering the best set of P_0, , P_+ and P_-. The maximum allowed deviation from the reference circle was $\Delta r = 3$ mm. The CMA-ES algorithm was run with 8 individuals in each generation and, the

analysis was run for 150 generations. The knockdown factors and critical stresses for this new design are shown in Table 7, in the column labelled "Simulation". This design was not tested experimentally and hence in the table there is no corresponding value under "Test".

Table 7: Knockdown factors and critical stresses for circular shell, Aster shell, and wavy shell, all made of nickel.

Shells	Knockdown Factor		Critical Stress [MPa]	
	Simulation	Test	Simulation	Test
Circular	0.362	0.753	74.895	155.618
Aster	0.895	0.774	216.174	187.118
Wavy	0.948	N/A	246.146	N/A

The critical stress values presented in Table 7 require some explanation. First, it can be seen that the "Test" value of the knockdown factor for the circular shell is unusually high, and in fact much higher than our estimate in the "Simulation" column. This suggests that the cylindrical shell was built very accurately, as confirmed by the measured imperfection amplitude of $0.1t$ (Araar, 1990). Second, the "Test" value of the knockdown factor for the Aster shell was 14% lower than the expected value in the "Simulation" column. This suggests that that there were significant imperfections in the as-built Aster shell, which is confirmed by the measured imperfection amplitude of $\sim 3t$ (Araar, 1990). Third, a comparison of the "Simulation" values of the knockdown factor for the Aster shell and our wavy shell design shows a 6% increase, even for a wavy shell design with only $N = 11$. In conclusion, this comparison indicates that Aster shells are difficult to build accurately and in any case our present design approach has even greater potential of eliminating imperfection sensitivity.

7. Mass Efficiency

A rational comparison between different architectures for cylindrical shell structures can be made in terms of the weight and load indices introduced in

Section 2.5. For circular cylinders the relationship between weight index and load index is provided by Eq. 9. For general cylindrical shells subject to axial compression, the relationship has the form:

$$\frac{W}{AR} = \frac{1}{\sqrt{\eta}}\sqrt{\frac{N_x}{R}} \tag{23}$$

where η is defined as the efficiency factor of the shell. Note that a larger value of η results in a higher load index for the same weight index.

The efficiency factor for monocoque cylindrical shells is obtained by comparing Eq. 23 with Eq. 9, and hence is given by:

$$\eta = \frac{\gamma E}{\rho^2\sqrt{3(1-\nu^2)}} \tag{24}$$

Equation 23 plots as a straight line of slope 0.5 in the log-log plot of weight index vs. load index, first shown in Fig. 7. Shells of equal efficiency lie on the same line, and therefore lines of slope 0.5 in this plot are called iso-efficiency lines.

Figure 23 is a revised version of Fig. 7 that shows, in addition to the original data, several results of the present study. The mirror-symmetric wavy shell with $N = 16$, which is the most efficient wavy shell design obtained so far, is shown in this plot together with its (dotted) iso-efficiency line. The efficiency factor for this design is 4.05 times that of perfect aluminum monocoque shells, and it can be seen in the plot that there are only three data points to the right of this line. Therefore, there are only three stiffened shells that beat the design $N = 16$: the fact that this design has higher efficiency than most existing stiffened shells is remarkable.

Several sinusoidally corrugated shells have also been included in Fig. 23. It is interesting to note that the data points corresponding to $k = 8, 10, 15$ go horizontally from left to right, but points corresponding to larger values of k lie on an iso-efficiency line and points corresponding to even larger values of N are further away from the line. It was already observed in Section 6.1 that there is a diminishing return in increasing k beyond 15, but it has now been shown that beyond $k = 15$ the mass efficiency actually begins to decrease.

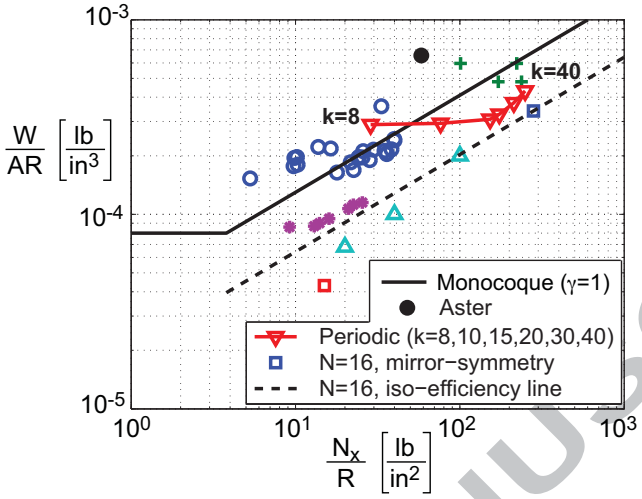

Figure 23: Revised version of Fig. 7 showing additional data points corresponding to mirror-symmetric wavy shell design with $N = 16$, sinusoidally corrugated shells, and Aster shell.

8. Conclusion

A novel structural form for monocoque cylindrical shells subject to axial loading has been proposed and an optimization technique to obtain geometric shapes that maximize the minimum between the buckling loads of the geometrically perfect structure and geometrically imperfect structures with positive and negative imperfections has been implemented. It has been shown that shell designs developed with this approach can achieve very high critical stress while also being practically insensitive to geometric imperfections.

Note that, because the critical buckling stress of an axially loaded cylindrical panel is inversely proportional to its radius of curvature, R, through $\sigma_{cl} \approx 0.6Et/R$, the large increase in the critical buckling stress that has been achieved by changing the cross-section of the shell from circular to either wavy or sinusoidally corrugated can be simply explained by the achieved reduction in the local radius curvature of the new designs.

A highlight of the present results is our design for a mirror-symmetric wavy shell with 16 independent control points, which has a knockdown factor 3.6

times that of a circular cylindrical shell with the same material properties and dimensions, and a critical buckling stress 10.8 times that of the circular cylindrical shell. Another highlight is that the present approach was able to generate a wavy cylinder design with knockdown factor and critical stress respectively 1.06 and 1.14 times those of a theoretical Aster shell based on Jullien and Araar (1991). Preliminary experimental validations of these results were presented in Ning and Pellegrino (2013) and a detailed study will be published in a follow-on paper.

It has also been shown that designs based on the present approach are comparable to the most efficient stiffened shell designs that have been developed during the past decades. These results appear very promising and justify further development of the proposed concept.

A comparison between the critical buckling modes of shell designs obtained from the present approach with the buckling modes of periodically corrugated shells has shown that optimized wavy cross-section designs are tuned to achieve highly localized modes, and this feature leads to superior performance. Our Fourier decompositions of each optimized cross-section into a series of periodic components indicate that wavy shells with better performance have both higher peak frequency and wider bandwidth, as well as more frequency components with larger amplitude. These results suggest that a systematic study of shell designs with increasing numbers of control points may be justified. It may lead to general trends in behavior that relate the relative magnitudes of the components with different wave numbers of the cross-section deviation from the reference circle to optimal or semi-optimal performance. These further development could then be exploited to develop future designs without going through a detailed optimization. Such follow-on work may also be advantageous in developing scaling techniques for shells with larger diameters, and particularly those with larger values of R/t.

A challenge associated with shells with larger diameters is that they will require cross-sections with a larger number of corrugations, in order to fully achieve their efficiency potential. It is possible, of course, to apply the present

analysis technique to such structures, but the number of nodes in the finite element analysis will scale linearly with the shell diameter, if the component wavelengths incorporated in the shell cross-section designs are not increased.

In concluding, two last points should be noted.

First, due to the non-convexity and lack of a mathematical expression for the present optimization problem, there is no guarantee that even a state of art optimizer for non-convex problems will converge to a global minimum. We have confirmed that our optimal design for a mirror-symmetric wavy shell with $N = 16$ is a local minimum by carrying out an additional gradient-based optimization with the fmincon function in MATLAB that used the CMA-ES optimum as an initial value. The improvement in the buckling load was less than 0.04%. Using a larger population size for the CMA-ES could increase the probability of obtaining global minima, but at the cost of increasing the computational time. A potential method to avoid a prohibitive increase in computations is to reduce the number of parameters needed to define the shape of the cross-section. Instead of using a NURBS interpolation through N control points, the cross-section could alternatively be described in terms of its Fourier spatial components, which would require fewer parameters than the 11 or 16 control points in the present study. As a result, the number of design variables in the optimization would be reduced and the probability of finding the global optimum would be increased, without increasing the population size.

Second, the present study has made the intuitive assumption that shells with non-straight generators would be less efficient. It would be interesting to further investigate this assumption.

Acknowledgements

We thank Professors J.-F. Jullien, P. Koumoutsakos, M.M. Mikulas and E. Ramm for help and advice during the course of this study. We also thank Professors C.R. Calladine, P. Ermanni, J. Hutchinson, K.-C. Park, T. Waas and P. Weaver for comments on a preliminary version of this study, presented

at the AIAA 54th SDM Conference. J. Steeves provided the lamina properties in Section 4.1. Financial support from the Resnick Institute at the California Institute of Technology is gratefully acknowledged.

References

References

Agarwal, B.L., Sobel, L.H., 1977. Weight Optimized Stiffened, Unstiffened, and Sandwich Cylindrical Shells. Journal of Aircraft 14, 1000-1008.

Araar, M., 1990. Contribution à L'autoraidissage des Coques Cylindriques vis-à-vis du Flambage. Thèse de Doctorat, INSA de Lyon.

Araar, M., Derbali, M., Jullien, J.F., 1998. Buckling of the Multi-Vaulted Aster Shell under Axial Compression Alone or Combined with an External Pressure. Structural Engineering and Mechanics 6(7), 827–839.

Arbocz, J., Babcock Jr, C.D., 1968. Experimental Investigation of the Effect of General Imperfections on the Buckling of Cylindrical Shells. NASA CR-1163.

Bäck, T., 1996. Evolutionary Algorithm in Theory and Practice: Evolution Strategies, Evolutionary Programming, Genetic Algorithms, Oxford University Press, Oxford.

Brush, D.O., Almroth, B.O., 1975. Buckling of Bars, Plates, and Shells, McGraw-Hill, New York.

Card, M.F., 1964a. Bending Tests of Large Diameter Cylinders Susceptible to General Instability. NASA TN D-2200.

Card, M.F., 1964b. Preliminary Results of Compression Tests on Cylinders With Eccentric Longitudinal Stiffeners. NASA TM X-1004

Card, M.F., Jones, R.M., 1966. Experimental and Theoretical Results for Buckling of Eccentrically Stiffened Cylinders. NASA TN D-3639.

Combescure, A., Pernette, E., 1989. Linear and Nonlinear Buckling of Discrete Supported Cooling Towers Using Special Axisymmetric Shell Elements. Nuclear Engineering and Design 111(2), 217-225.

Daniel, I.M., Ishai, O., 2006. Engineering Mechanics of Composite Materials, Oxford University Press, Oxford.

Davis, R., 1982. Buckling Test of a 3-Meter-Diameter Corrugated Graphite-Epoxy Ring-Stiffened Cylinder. NASA TP-2032.

Donnell, L.H., Wan, C.C., 1950. Effects of Imperfections on Buckling of Thin Cylinders and Columns under Axial Compression. Journal of Applied Mechanics 17, 73-83.

Elishakoff, I., 2012. Probabilistic Resolution of the Twentieth Century Conundrum in Elastic Stability. Thin-Walled Structures 59, 35-57.

Hansen, N., Müller, S.D., Koumoutsakos, P., 2003. Reducing the Time Complexity of the Derandomized Evolution Strategy with Covariance Matrix Adaptation (CMA-ES). Evolutionary Computation 11, 1-18.

Hansen, N., 2011. The CMA Evolution Strategy: A Tutorial.

Hansen, N., 2012. The CMA Evolutionary Strategy. Downloaded from https://www.lri.fr/ hansen/cmaesintro.html on December 12, 2012.

Hilburger, M.W., Starnes, J.H, 2001. High-Fidelity Nonlinear Analysis of Compression-Loaded Composite Shells. AIAA Paper 2001-1394.

Hilburger, M.W, Nemeth, M.P., Starnes, J.H., 2006. Shell buckling Design Criteria Based on Manufacturing Imperfection Signatures. AIAA Journal 44, 654-663.

Hughes, T.J.R., Cottrell, J.A., Bazilevs, Y., 2009. Isogeometric Analysis: CAD, Finite Elements, NURBS, Exact Geometry and Mesh Refinement. Wiley, New York.

Hutchinson, J.W., Koiter, W.T., 1970. Postbuckling Theory. Applied Mechanics Reviews 23, 1353-1366.

Jones, R.M., 2006. Buckling of Bars, Plates, and Shells, Bull Ridge, Blacksburg.

Jullien, J.F., Araar, M., 1991. Towards an Optimal Cylindrical Shell Structures under External Pressure, in: Jullien, J.F., Buckling of Shell Structures, on Land, in the Sea, and in the Air. Elsevier, London, pp. 21-32.

Katz, L., 1965. Compression Tests on Integrally Stiffened Cylinders. NASA TM X- 53315.

Koiter, W.T., 1945. On the Stability of Elastic Equilibrium. thesis(in Dutch with English summary), Delft, H. J. Paris, Amsterdam. English translation, Air Force Flight Dym. Lab. Tech. Rep., AFFDL-TR-70-25.

Koiter, W.T., 1963. The Effect of Axisymmetric Imperfections on the Buckling of Cylindrical Shells under Axial Compression. Proc. K. Ned. Akad. Wet., Amsterdam, ser. B, vol. 6; also, Lockheed Missiles and Space Co. Rep. 6-90-63-86, Palo Alto, California.

Nemeth, M., Mikulas, M.M., 2009. Simple Formulas and Results for Buckling-Resistance and Stiffness Design of Compression-Loaded Laminated-Composite Cylinders. NASA TP-2009-215778.

Nemeth, M.P., Starnes, J.H., 1998. The NASA Monographs on Shell Stability Design Recommendations: a Review and Suggested Improvements. NASA TP-1998-206290.

Ning, X., Pellegrino, S., 2013. Imperfection-Insensitive Axially Loaded Cylindrical Shells. 54th AIAA/ASME/ASCE/AHS/ASC Structures, Structural Dynamics and Materials Conference. 8-11 April 2013, Boston, MA, AIAA-2013-1768.

Peterson, J.P., Seide, P., Weingarten, V.I., 1965. Buckling of Thin-Walled Circular Cylinders. NASA SP-8007.

Peterson, J.P. , 1967. Structural Efficiency of Ring-Stiffened Corrugated Cylinders in Axial Compression. NASA TN D-1073.

Ramm, E., Wall, W.A., 2004. Shell Structures − a Sensitive Interrelation between Physics and Numerics. International Journal for Numerical Methods in Engineering 60, 381-427.

Reitinger, R., Bletzinger, K.U., Ramm, E., 1994. Shape Optimization of Buckling Sensitive Structures. Computing Systems in Engineering 5, 65-75.

Reitinger, R., Ramm, E., 1995. Buckling and Imperfection Sensitivity in the Optimization of Shell Structures. Thin-walled structures 23, 159-177.

Rotter, J.M., Coleman, R., Ding, X.L., Teng, J.G., 1992. The Measurement of Imperfections in Cylindrical Silos for Buckling Strength Assessment. In: Proceedings of 4th International Conference on Bulk Materials, Storage, Handling and Transportation, Wollongong, Australia, 473-479.

Scott, N.D., Harding, J.E., Dowling, P.J., 1987. Fabrication of Small Scale Stiffened Cylindrical Shells. Journal of Strain Analysis 22, 97-106.

Singer, J., Arbocz, J., Weller, T., 2002. Buckling Experiments: Experimental Methods in Buckling of Thin-Walled Structures: Vol. 2, Wiley, New York.

Teng, J.G., 1996. Buckling of Thin Shells: Recent Advances and Trends. Applied Mechanics Reviews, 49(4), 263-274.

Thompson, J.M.T., 1972. Optimization as a Generator of Structural Instability. International Journal of Mechanical Sciences 14, 627-629.

Von Kármán, T., Tsien, H.S., 1941. The Buckling of Thin Cylindrical Shells under Axial Compression. Journal of the Aeronautical Sciences 8, 303-312, 1941.